



Supporting Information

for *Small*, DOI: 10.1002/smll.202204693

Continuous Flow Microfluidic Production of Arbitrarily
Long Tubular Liquid Crystal Elastomer Peristaltic Pump
Actuators

*Najiya Najiya, Nikolay Popov, Venkata Subba Rao
Jampani, and Jan P. F. Lagerwall**

Supporting information

S1 Calculation of average linear flow rates

To analyze the flow profile, we first measure the radius of each phase p in the tubular jet to calculate the cross section area A_p of each phase, and then we obtain the average linear flow rates in the three phases as $\bar{v}_p = \phi_p/A_p$. We do this analysis for one of the experiments in which LCE tubes were made by UV-crosslinking, an excerpt of the tubular flow shown in Fig. S1a. The jet is slightly asymmetric, the outer and middle phases appearing slightly thicker at the top than at the bottom of the photo. We attribute this to a slight asymmetry in the coaxial capillary device and assume, for simplicity, that all boundaries between the phases remain circular, albeit not quite coaxial, as schematically illustrated in Fig. S1b.

The cross section area of the inner phase is easily obtained as $A_i = \pi r_i^2 \approx \pi \cdot 0.1238^2 \approx 0.0482 \text{ mm}^2$, where $r_i \approx 0.1238 \text{ mm}$ is the radius of the inner phase in the jet, as obtained from the measured inner diameter (green double arrow) in Fig. S1a. For the middle phase, the corresponding cross section is given by $A_m = \pi r_m^2 - A_i$, where r_m is the outer radius of the middle phase, obtained as half the corresponding diameter (red double arrow) measured in the same photo. We thus obtain $A_m \approx \pi \cdot 0.155^2 - 0.0482 \approx 0.0273 \text{ mm}^2$. Finally, the outer phase cross section area is obtained analogously as $A_o = \pi r_o^2 - A_m - A_i$, with r_o the inner radius of the collection capillary, obtained as half the blue double-headed diameter measured in the same photo. This yields $A_o \approx \pi \cdot 0.29^2 - 0.0273 - 0.0482 \approx 0.1887 \text{ mm}^2$.

With volumetric flow rates of $\phi_i = 4.0 \text{ mL/h}$, $\phi_m = 2.0 \text{ mL/h}$ and $\phi_o = 8.0 \text{ mL/h}$ these cross sections yield average linear flow velocities of $\bar{v}_i = \phi_i/A_i \approx 4.0 \cdot 10^3/3600/0.0482 \approx 23.1 \text{ mm/s}$, $\bar{v}_m = \phi_m/A_m \approx 2.0 \cdot 10^3/3600/0.0273 \approx 20.4 \text{ mm/s}$ and $\bar{v}_o = \phi_o/A_o \approx 8.0 \cdot 10^3/3600/0.1887 \approx 11.8 \text{ mm/s}$. Based on these values we estimate the flow velocity profile sketched in Fig. S1c, illustrating that the LCO solution is being sheared between the inner phase, flowing at maximum \bar{v} , and the outer phase, exhibiting the lowest \bar{v} . Note that the overall flow profile is only a rough estimate; it satisfies the no-slip boundary conditions at each interface and the average flow velocity within each phase, but the exact variation of velocity across each phase has not been calculated.

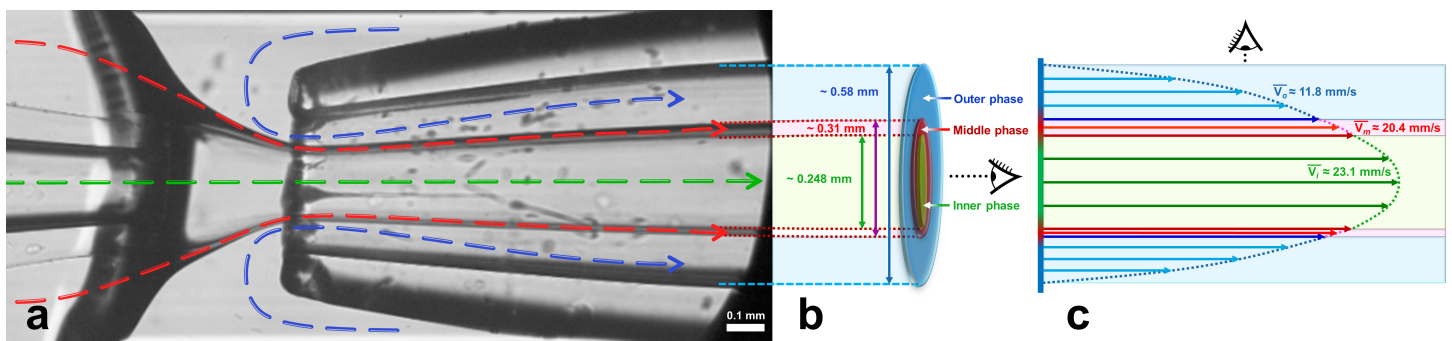


Figure S1: (a) Example screenshot of LCE tube production with schematic arrows showing flow directions of the inner, middle, and outer phase in green, red and blue, respectively, (fluids as in Fig. 3, lower row). The following volumetric flow rates are set: $\phi_i = 4.0 \text{ mL/h}$, $\phi_m = 2.0 \text{ mL/h}$ and $\phi_o = 8.0 \text{ mL/h}$. The average flow velocities are calculated to estimate the overall flow profile. The average flow velocities are taken into account after a minor extrapolation (b), where the coaxial tubular flow reached its nearly maximum diameter. (b) Schematic of the composite flow cross-section, with inner, middle and outer phases in green, red and blue, respectively. (c) Estimated flow profile corresponding to the average velocities obtained from (a) and (b), indicated on the right. The flow profile is estimated, and each phase's average arrow length corresponds to its approximate average velocity. The overall flow profile shows it to be a nearly narrow parabolic shape, representing a laminar flow, despite slight asymmetry and uneven wall thickness of the tubular flow of the middle phase. Asymmetry could happen due to the resulting non-ideal straight perpendicular cutting of cylindrical glass capillaries in the microfluidic capillary device for this case.

S2 Spectroscopic confirmation that oligomers have acrylate end groups required for polymerization

Infrared spectra were recorded in transmission using a Nicolet IS5 FTIR spectrophotometer equipped with a diamond attenuated transmission reflectance (ID7-ATR) device. The samples were analyzed across the region 4000 to 500 cm^{-1} with 16 scans with a nominal resolution of 4 cm^{-1} using OMNIC software by Thermo Fisher Scientific. LCO1 and LCO2 samples were dissolved in DCM for the experiment. The spectra are shown in Supplementary Fig. S2.

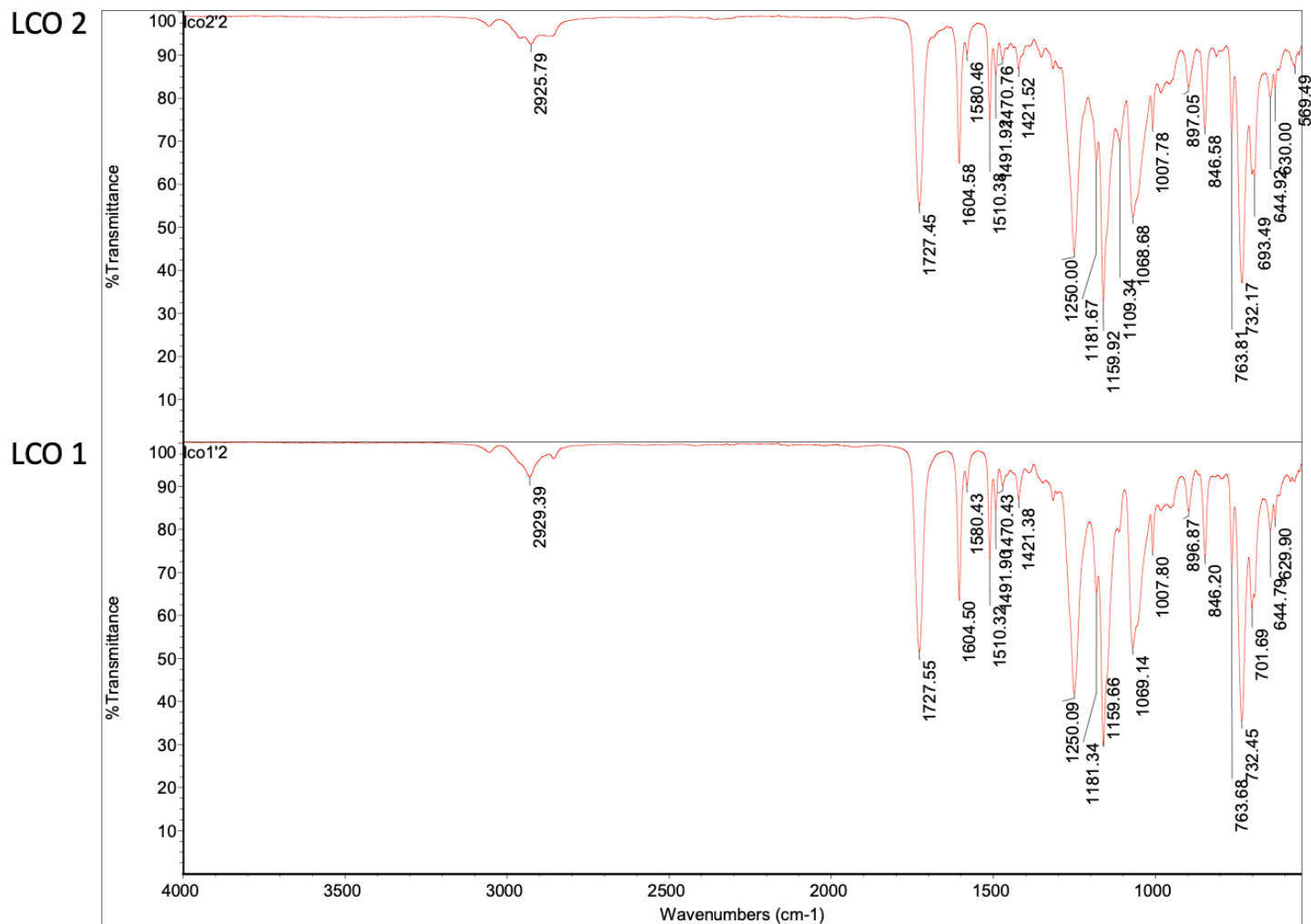


Figure S2: IR spectra of LCO1 and LCO2 precursor solutions in DCM.

The absence of peaks at 2600-2500 cm^{-1} in both spectra confirms the absence of free thiol in LCO1 and LCO2, which in turn implies that the chain extender is completely reacted during the oligomer synthesis. The out-of-plane C-H bending vibrations in the range 885-800 cm^{-1} indicates the presence of acrylate groups at the end.

S3 Mechanical testing of LCE tubes

For the tensile strain-stress experiments, the tube under testing was mounted vertically in a Mark-10, F105-IMTE Advanced Test Frame, coupled with FS05-05 Tension and Compression Force Sensors (maximum load of 0.5 N), fixing its ends using tape. The tensile strain along the tube is defined as $\epsilon = \frac{\Delta L}{L_0}$, where ΔL is the length extension and L_0 is the original tube length, prior to starting the experiment. The tensile stress was calculated as $\sigma = F/a$, where a is the dynamic cross-sectional area of the tube

and F is the force measured by the instrument. The original cross-sectional area a_0 was measured using the POM (Olympus), and the dynamic value during the experiment was calculated as $a = \frac{L_0 A_0}{\Delta L + L_0}$. The original cross-sectional area of the LCE tube was $a_0 \approx 0.07 \text{ mm}^2$. The data obtained during experiments on three different sections of a pristine tube, each stretched until rupture, are shown in Supplementary Fig. S3.

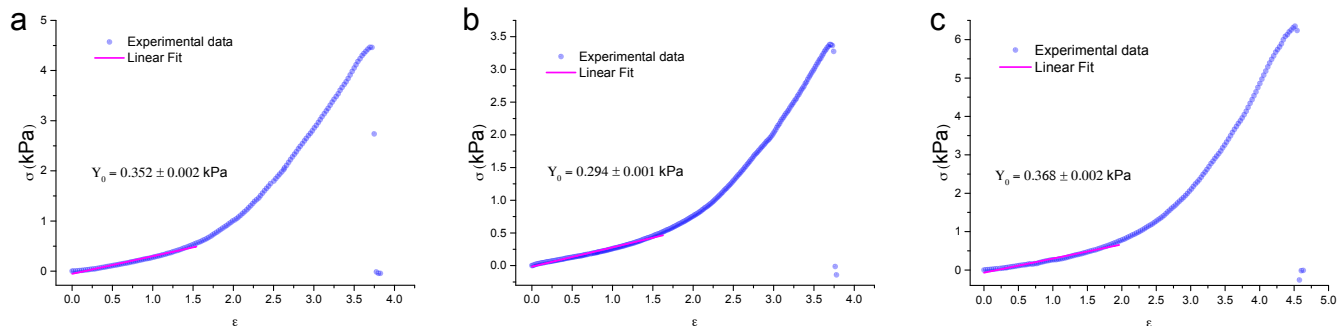


Figure S3: Stress σ versus engineering strain ϵ of an LCO₂-based LCE tube upon stretching until breaking, measured in three different sections of the same tube.

S4 Confirmation of continuous hollow core

In this experiment, we connect one end of a 21 cm long LCE tube to a glass capillary that has been tapered using the Sutter Instrument P-1000 micropipette puller, followed by cutting off the end with the Narishige MF-900 microforge until its smallest orifice has an outer diameter of about $100 \mu\text{m}$. This allows us to thread the LCE tube over the tapered end. The other end of the capillary is connected to a PTFE microtubing which is connected to a syringe filled with Congo Red-dyed water at its other end via a standard Luer lock connector. This whole set-up is mounted on a pole vertically, with a Petri dish below the lower tube orifice, as shown in Supplementary Fig. S4a and Supplementary Video 5.

The piston of the syringe is now pressed slowly to push the red-dyed water through the tube. As the water moves through the tube, it becomes red-colored (Fig. S4), and then the liquid emerges as a droplet at the lower orifice (Fig. S4)c). Pressing the plunger further, more and more red-dyed water passes through the tube, being collected in the Petri dish, as also shown in Supplementary Video 5. Given the $300 \mu\text{m}$ diameter of the tube, this proves a hollow core continuity across a length of nearly 800 diameters. We consider this an acceptable demonstration that the tubular structure is continuous with respect to its hollow core.

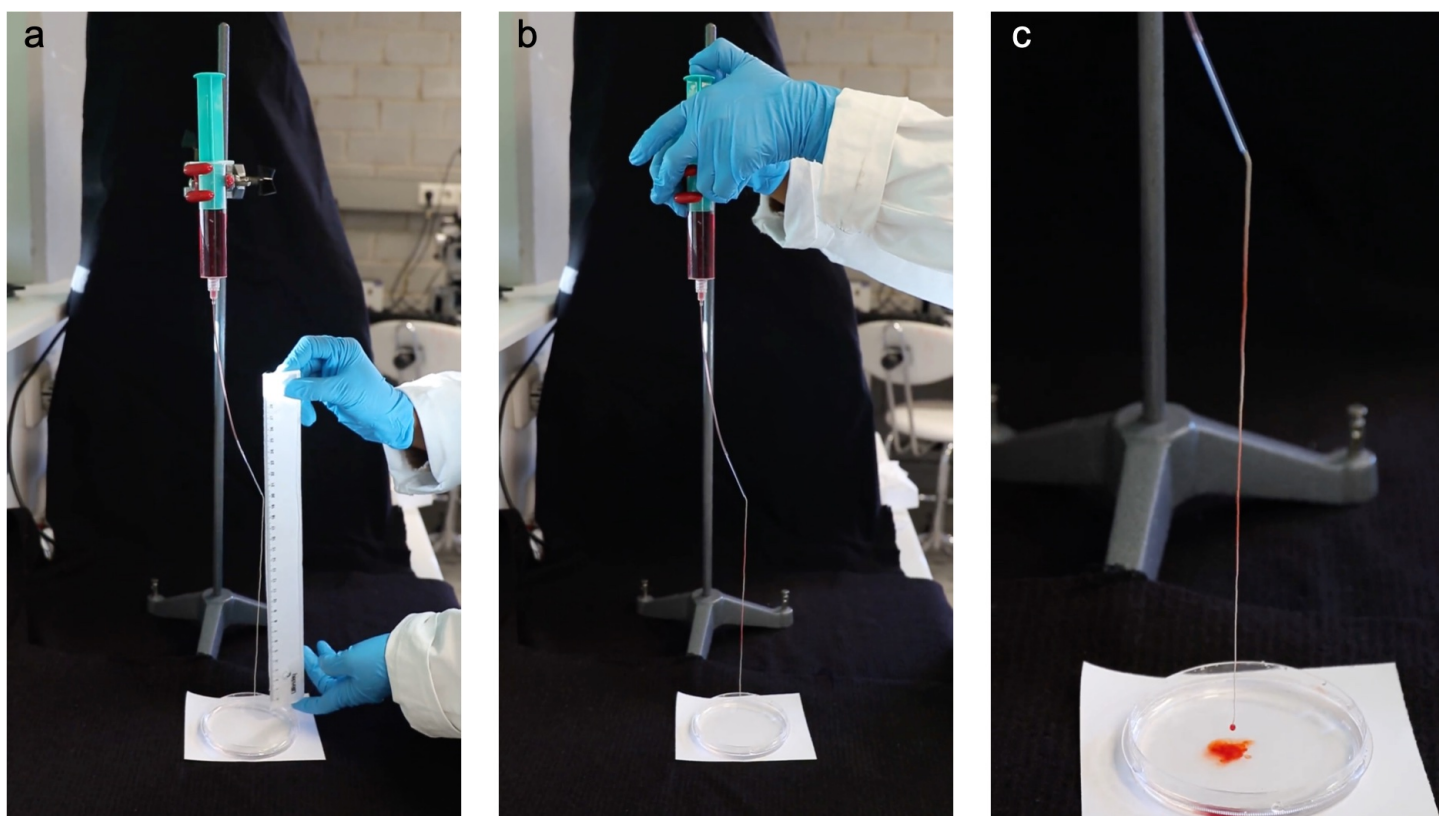


Figure S4: Experimental set-up for pumping liquid through an LCE tube section